


Article

The Longitudinal Effect of Meditation on Resting-State Functional Connectivity Using Dynamic Arterial Spin Labeling: A Feasibility Study

Zongpai Zhang ¹, Wen-Ming Luh ², Wenna Duan ¹, Tony D. Zhou ¹, Li Zhao ³ , George Weinschenk ¹, Adam K. Anderson ⁴ and Weiyong Dai ^{1,*}

¹ Department of Computer Science, State University of New York at Binghamton, Binghamton, NY 13902, USA; zzhan145@binghamton.edu (Z.Z.); wduan1@binghamton.edu (W.D.); tonyzhou.mp@gmail.com (T.D.Z.); weinscgg@binghamton.edu (G.W.)

² National Institute on Aging, National Institutes of Health, Baltimore, MD 21225, USA; wenming.luh@nih.gov

³ College of Biomedical Engineering & Instrument Science, Zhejiang University, Hangzhou 310027, China; lz5bf@virginia.edu

⁴ Department of Human Development, Cornell University, Ithaca, NY 14853, USA; aka47@cornell.edu

* Correspondence: wdai@binghamton.edu; Tel.: +1-(607)-777-4859

Abstract: We aimed to assess whether dynamic arterial spin labeling (dASL), a novel quantitative MRI technique with minimal contamination of subject motion and physiological noises, could detect the longitudinal effect of focused attention meditation (FAM) on resting-state functional connectivity (rsFC). A total of 10 novice meditators who recorded their FAM practice time were scanned at baseline and at the 2-month follow-up. Two-month meditation practice caused significantly increased rsFC between the left medial temporal (LMT) seed and precuneus area and between the right frontal eye (RFE) seed and medial prefrontal cortex. Meditation practice time was found to be positively associated with longitudinal changes of rsFC between the default mode network (DMN) and dorsal attention network (DAN), between DMN and insula, and between DAN and the frontoparietal control network (FPN) but negatively associated with changes of rsFC between DMN and FPN, and between DAN and visual regions. These findings demonstrate the capability of dASL in identifying the FAM-induced rsFC changes and suggest that the practice of FAM can strengthen the efficient control of FPN on fast switching between DMN and DAN and enhance the utilization of attentional resources with reduced focus on visual processing.

Keywords: meditation; functional magnetic resonance imaging; functional connectivity; arterial spin labeling; default mode network; dorsal attention network



Citation: Zhang, Z.; Luh, W.-M.; Duan, W.; Zhou, T.D.; Zhao, L.; Weinschenk, G.; Anderson, A.K.; Dai, W. The Longitudinal Effect of Meditation on Resting-State Functional Connectivity Using Dynamic Arterial Spin Labeling: A Feasibility Study. *Brain Sci.* **2021**, *11*, 1263. <https://doi.org/10.3390/brainsci11101263>

Academic Editor: Charles F. Geier

Received: 19 July 2021

Accepted: 20 September 2021

Published: 24 September 2021

Publisher's Note: MDPI stays neutral with regard to jurisdictional claims in published maps and institutional affiliations.



Copyright: © 2021 by the authors. Licensee MDPI, Basel, Switzerland. This article is an open access article distributed under the terms and conditions of the Creative Commons Attribution (CC BY) license (<https://creativecommons.org/licenses/by/4.0/>).

1. Introduction

Meditation provides evidence of a diverse set of benefits, including emotional regulation [1], awareness and self-regulation [2], memory and cognition [3], attention [4], and working memory [5]. Meditation has also been demonstrated to be beneficial to the treatment of psychological disorders [6–9]. Neuroimaging studies have examined the state effect and the trait effect of meditation. The state effect refers to the short-term consequences during an individual's meditative practice. The trait effect characterizes the long-lasting changes that accrue via repetitive practice even when the meditation is not practiced. The therapeutic effects and daily life benefits (e.g., improved attention) emerge from the trait-related brain changes that are induced by meditation.

Meditation has been associated with trait changes of the brain structure using cross-sectional structural magnetic resonance imaging (sMRI) studies. Increased gray matter (GM) density [10–12] and cortical thickness [13–16] have been found in the default mode network (DMN) and dorsal attention network (DAN) regions in charge of self-referential and attention processing: such as superior parietal gyri (a posterior region in DAN),

precuneus (a posterior region in DMN), anterior cingulate, superior and middle frontal gyri, and orbitofrontal (prefrontal regions in DMN) regions in meditators. Longitudinal sMRI studies further confirmed causal effects of meditation on increased GM density after an 8-week meditation training in the posterior cingulate cortex and temporoparietal junction (posterior regions in DMN) [15,17,18]. Therefore, we hypothesized that meditation would result in altered brain resting-state functional connectivity (rsFC) with key regions of DMN (posterior cingulate cortex (PCC) and ventromedial prefrontal cortex (vmPFC)) and DAN (left middle temporal (LMT), right middle temporal (RMT), left frontal eye (LFE), right frontal eye (RFE), left superior parietal lobule (LSPL), and right superior parietal lobule (RSPL)) [19] and that the changes are correlated with meditation practice time. In a recent study on the same subjects used in the present work, we have found that meditation can significantly increase rsFC between DMN and DAN [20].

The trait-related brain changes have been studied for the neural basis underlying the experience and training predominantly using blood-oxygen-level-dependent (BOLD) resting-state functional MRI (rsfMRI) [21]. Recent studies focused on understanding the effects of meditation on patterns of rsFC across distributed brain regions or networks (for a review, see [22]). The studies have provided ample evidence that meditation training alters brain rsFC and the changes of rsFC are associated with the duration of meditation experience. However, the recent literature review indicated few converging findings on the meditation effects on functional connectivity (FC) [22].

Pseudo-continuous arterial spin labeling (PCASL) [23] provides a noninvasive way of measuring three-dimensional (3D) cerebral blood flow (CBF). Recently, dynamic arterial spin labeling (dASL) [24], which measures rsFC by collecting a time series of CBF images, can detect brain resting-state networks without artifactual “networks” that are typically detected in BOLD studies prior to subjective filtering. BOLD rsfMRI signals consist of motion artifacts and physiological noises, including head motion, cardiac pulsation, and respiratory motion [25,26]. For example, increased head motion can increase the long-distance rsFC but decrease short-distance rsFC. It is possible that experienced meditators may exhibit less head motion within the scanner and slower cardiac and respiratory rates, especially during some meditation tasks, and the acquisition method should therefore account for possible differences from the factors. By contrast, dASL has the advantage of minimal influence from small motion artifacts and physiological noises because it can be combined with the other background suppression techniques to suppress the background tissue signals. dASL is sensitive to subject motion due to the subtraction of label and control images. Motion-induced static tissue signal changes cause imperfect subtraction and hence motion artifacts in the ASL difference images. Strong background suppression markedly reduces static tissue signals and therefore motion artifacts (i.e., motion-induced subtraction errors). This advantage is particularly relevant to meditation researches as frequent changes in the peripheral physiology of respiration and heart rate can markedly affect the detection of fMRI signals and estimates of functional connectivity. In addition, we have demonstrated that dASL with 3D fast spin-echo (FSE) image acquisition has minimal air-tissue susceptibility artifacts in areas such as the orbitofrontal cortex (OFC) and medial/inferior temporal cortex [24]. Hence, the background suppression of PCASL time series with 3D FSE readout can provide better sensitivity for probing rsFC with the susceptibility regions. Therefore, dASL is expected to be more sensitive in detecting the rsFC changes caused by meditation practice. The dASL time-series acquisition can quantify time-averaged CBF in an absolute physiological unit (mL/100 g·min) besides the measurement of rsFC. Additionally, it is unclear whether the trait-related changes are actually caused by the duration of meditation practice despite the reported association of meditation practice time with rsFC between brain regions or networks [27–30]. These findings may be caused by not accounting for baseline rsFC before performing the meditation. Herein, we chose a longitudinal study (to remove the effect of baseline rsFC) to investigate the feasibility and sensitivity of dASL in detecting the effects of meditation on rsFC and CBF. Considering the regulatory role of frontoparietal control network (FPN)

in the attention control in response to salient stimuli [31,32] and consistent finding for inter-network connections among DMN, FPN, and salience network (SN) during active meditation state [33–36], we anticipated that dASL is capable of detecting rsFC with FPN and SN from DMN and DAN seeds. Given that there are many different forms of meditation, such as focused attention or open monitoring or non-dual awareness, we studied one specific type of meditation—focused attention meditation (FAM)—in the study to avoid potentially canceling effects from different meditation categories.

2. Methods

2.1. Sample Size Justification

Based on the increased PCC rsFC [37] after weeks of meditation training, we have previously derived an effect size of 0.81 with conventional BOLD [20]. Our dASL method increases the effect size by 49% for the ACC rsFC in bipolar disorder patients, compared to conventional BOLD fMRI [38]. However, the effect size of rsFC is dependent on the seed locations. Assuming that the maximum increase in the effect size for ACC rsFC is reached for the dASL method, we can consider the effect size of dASL increases by about half of 49% (i.e., 24%) on average from conventional BOLD. To detect a meditation effect size of 1.00 using dASL (24% of the expected increase in the effect size with the dASL method from the effect size of 0.81 with conventional BOLD) between the baseline and follow-up, a sample size of 9 is required to achieve a power of 80% and a level of significance of 5%. This study had an actual sample size of 10, which provides sufficient power to detect the meditation effect using the dASL method.

2.2. Study Population

A total of 11 healthy undergraduates at the Binghamton University (5 females, mean age: 19.09 ± 0.54 years, age range: 19 to 20 years) participated in the study. All participants were recruited from a university-offered meditation course. Nine participants had no prior meditation experience before, while two participants had a brief meditation period without any specific guidance in their prior yoga classes.

The meditation course introduced several different types of meditation techniques and reviewed the benefit of meditation on behaviors from literature. The instructor guided students for 15 min meditation once or twice per week during class in order to have students familiar with different meditation styles. Participants were instructed during class to sit comfortably, relax shoulders, close/open eyes, concentrate on a selected point focus (e.g., breath), and repeatedly bring the attention back to the selected focus if they noticed their attention had drifted. Participants could choose their own point of focus during the meditation practice, such as their breath, a spot on the wall, a phrase, or anything else they felt appropriate. Homework required practice FAM for at least 10 min per session and no less than 5 times per week and writing a weekly journal by describing their practice experiences.

All 11 participants underwent the baseline MRI scans before any homework assignments. One subject was not able to attend the follow-up scan after 2 months. Participants reported their total practice time according to their daily logs between the baseline and follow-up scans. The total practice time was calculated as the sum of all meditation practice time, including those from class and homework practice.

2.3. MRI Acquisition

We scanned meditation participants, including 11 at baseline and 10 at the 2-month follow-up, on a 3 Tesla GE MR750 scanner (General Electric, Milwaukee, WI, USA) using a 32-channel receive-only phased-array head coil at Cornell University MRI Facility. The Institutional Review Board of Cornell University approved the study, and all participants fully understood and signed written informed consent. All methods described in this manuscript were performed in strict accordance with the approved guidelines. The scans included 3D whole-brain sagittal T1-weighted magnetization prepared rapid gradient

echo (MPRAGE) images for image registration, and the resting-state 3D dynamic arterial spin labeling (dASL), specifically, MPRAGE images were acquired in 5 min 30 s with the following parameters: field of view (FOV): 25 cm, 176 slices with matrix size: 256×256 ; slice thickness: 1.0 mm, repetition time (TR): 7 ms, echo time (TE): 3.42 ms, inversion time (TI): 425 ms, flip angle: 70, receiver bandwidth (rBW): 25 kHz. The pseudo-continuous arterial spin labeling (PCASL) sequence [24] was used to label the blood. The labeling duration was 2 s, with a delay of 1.8 s after labeling. Optimized background suppression pulses achieved less than 0.3% of background signals [24,39]. We acquired 50 3D dASL whole-brain volumes and a reference volume in 17 min. The reference volume was used for perfusion quantification. Each ASL volume, requiring a control-label pair and two spiral interleaves, was obtained with a 3D stack of spirals RARE sequence in a duration of 20 s.

2.4. Image Processing

2.4.1. Quantification of Absolute CBF Maps

Reconstruction of the ASL label-control difference image time series was obtained by our custom reconstruction algorithm [24,40]. The first 3D ASL difference image was removed to increase stability for further processing. The head motion was corrected by realigning the remaining ASL image time series after which the average of the head-motion corrected images were generated. The average absolute CBF map for each subject was quantified using the standard kinetic model [41–43] with the mean of the head-motion-corrected ASL images and the reference image.

2.4.2. Normalization of dASL Image Time Series and CBF Maps

For each subject, the motion-corrected ASL image time series were transformed to the standard MNI brain space. Specifically, GM, white matter, and cerebrospinal fluid probability maps were generated by segmenting high-resolution MPRAGE images. The GM probability maps were co-registered to the average of motion-corrected ASL images. The motion-corrected ASL time series and the average CBF map for each subject were transformed into the standard space by applying the same transformation that was obtained by the normalization from the co-registered GM probability map to the prior GM template in standard brain space. To correct for global CBF differences in the longitudinal setting, the relative CBF map for each subject was calculated by dividing the global mean CBF signal. The relative CBF was used because it was reported to be more sensitive in statistical analyses for group comparisons [44].

2.4.3. Quantification of CBF Functional Connectivity Maps

Due to the minimal contamination from motion artifacts and physiological noises, the dASL image time series were not processed for removing the noises. Global CBF values, averaged over the whole brain, were regressed out from the dASL image time series. Eight seeds were chosen from the default mode network (DMN) and dorsal attention network (DAN). Two seeds were from DMN: the posterior cingulate cortex (PCC) and the ventromedial prefrontal cortex (vmPFC). Six seeds were from DAN: the left middle temporal area (LMT), the right middle temporal area (RMT), the left frontal eye field (LFE), the right frontal eye field (RFE), the left superior parietal lobule (LSPL), and the right superior parietal lobule (RSPL). The seeds were chosen to cover different anatomical extents: frontal cortex, parietal cortex, and temporal cortex. All seed regions of interest (ROIs) were defined as a sphere with a volume of $\sim 2 \text{ cm}^3$. The centers of the seed ROIs were selected from a previous study [19] (see a summary in Figure 1) that examined the spatial distribution of DMN and DAN. For each subject, a CBF rsFC map with a seed ROI was calculated as voxel-wise Pearson correlation coefficients between the dASL time series and the time series of each seed ROI. All Individual CBF rsFC maps with all seed ROIs were transformed into z score maps by using a Fisher z transformation to improve normality for group-level comparisons.

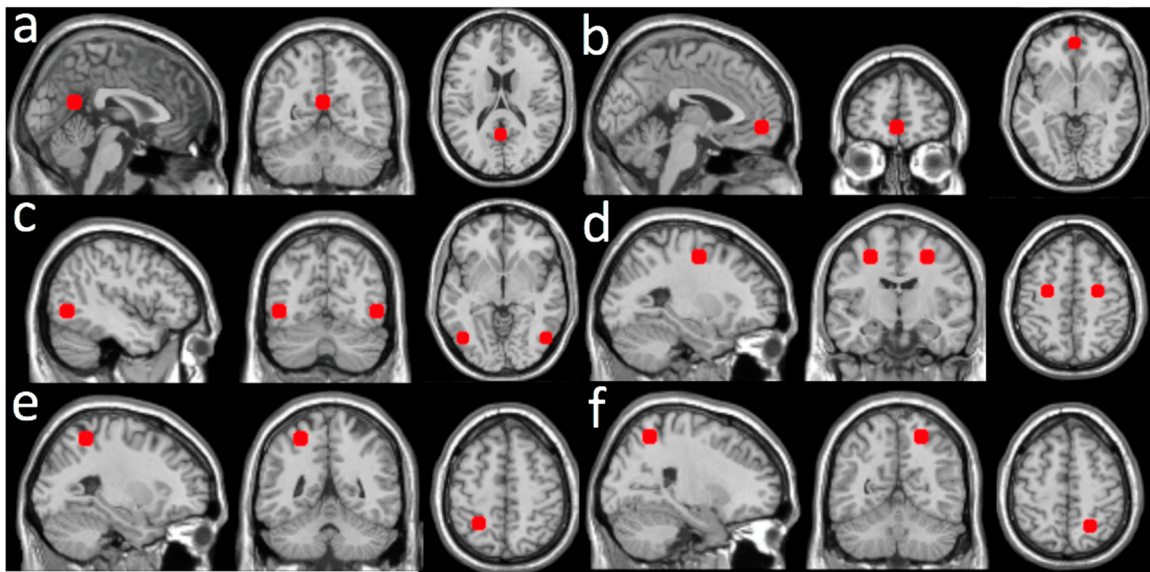


Figure 1. ROIs constructed from the seeds with the MNI coordinates listed: (a) posterior cingulate cortex (PCC, (1, −55, 17) mm); (b) ventromedial prefrontal cortex (PFC, (0, 51, −7) mm); (c) left and right middle temporal area (LMT, (−45, −69, −2) mm and RMT, (50, −69, −3) mm); (d) left and right frontal eye fields (LFE, (−25, −8, 50) mm and RFE, (27, −8, 50) mm); (e) left superior parietal lobule (LSPL, (−27, −52, 57) mm); (f) right superior parietal lobule (RSPL, (24, −56, 55) mm).

2.5. Statistical Analysis

The relative CBF maps and z-score maps from all seed ROIs in the standard space were smoothed with a $6 \times 6 \times 6 \text{ mm}^3$ Gaussian kernel. In order to evaluate the changes of CBF measures from the baseline to 2-month follow-up, the z score maps, and relative CBF maps were modeled, respectively, using SPM12 via general linear model (GLM). In the GLM, the z score maps from each seed (and the relative CBF maps) were used as the dependent variables. The status index (baseline or follow-up), subject index (whether two scans are from the same subject or not), and gender were used as the independent variables. Age was not used as a covariate because the participants had a maximum of a 1-year age difference. The voxel-level significance threshold was set to $p < 0.005$. A cluster-level p -value of 0.05 was used to correct for multiple comparisons that were controlled by family-wise error (FWE). A more liberal voxel-level p -value threshold of 0.01 and FWE-corrected cluster-level p -value threshold of 0.05 were also used to view the trend if the above stringent p values failed to detect the longitudinal effects of meditation. The automated anatomical labeling (AAL) atlas binary mask was used to analyze only the GM regions.

To investigate the association of the longitudinal changes in CBF measures with meditation practice time, the difference of the z-score maps and relative CBF maps between the baseline and follow-up was modeled using SPM12 via GLM. In GLM, the difference maps from each contrast were used as the dependent variables. Gender and practice time were used as independent variables. The voxel-level p -value and FWE-corrected cluster-level p -value thresholds were set as 0.005 (more liberal value of 0.01 later to view the trend) and 0.05.

Post hoc regional analyses were performed to visualize the longitudinal changes and the relationship between the longitudinal changes and meditation practice time in those CBF measures. The significant clusters obtained from either voxel-based analysis were separated into different ROIs. The regional value for each ROI was calculated as the mean signal value over all the voxels within the region. Post hoc regional analyses were performed using paired t -test with gender as a covariate and multiple linear regression analysis with gender and meditation practice time as covariates, respectively.

3. Results

3.1. Basic Characteristics of the Participants

Table 1 summarizes the participants' information and meditation practice time. One participant was not scanned at follow-up. The meditation practice duration and practice time for the remaining ten participants is 66.50 ± 4.14 days and 574.00 ± 465.55 min. Only 10 participants were included in the longitudinal analysis. Among them, two had practice time of more than 1000 min.

Table 1. Summary of demographical characteristics and meditation practice time.

	At Follow-Up
Total number of included subjects *	10
Age range	19 years (8), 20 years (2)
Gender	Male (6), Female (4)
Handedness	Right (7), Left (3)
Total practice time (minutes)	Range: (135, 1620) 574 ± 465
Time duration (days)	Range: (45, 72) 66 ± 4

* One subject was excluded because of not being scanned at follow-up.

3.2. Quality of dASL Time Series

dASL image time series was of good quality. Representative dASL images from four random time points and their temporal signal-to-noise ratio (SNR) map across all time points are shown in Supplementary Figure S1. The temporal SNR map for each subject was calculated as the mean dASL image divided by the standard deviation map across all time points. The GM temporal SNR value for each dASL scan was calculated by averaging the temporal SNR map over the GM ROI. GM ROI was defined as the voxels that have over 60% of probability in the SPM12 tissue probability map. The average temporal SNR value across 10 subjects was 7.83 ± 1.19 at the baseline and 7.65 ± 0.97 at follow-up.

3.3. Differences in Global CBF and Relative CBF between the Baseline and Follow-Up

No significant global CBF changes ($p = 0.52$) were found after correcting for gender effects from the baseline to follow-up. No significant relative CBF changes were observed from the baseline to follow-up using a voxel-level $p < 0.005$. With a liberal voxel-level $p < 0.01$, we observed a relative CBF increase in the junction of occipital, temporal and parietal regions (corrected cluster-level $p = 0.027$) (Supplementary Figure S2a) and a relative CBF decrease primarily in the thalamus region (corrected cluster-level $p = 0.002$) (Supplementary Figure S2b) at follow-up, compared to the baseline. A summary of the two clusters' statistics is listed in Supplementary Table S1.

3.4. Association of Relative CBF with Meditation Practice Time

No significant relative CBF changes were observed to associate with meditation practice time from the baseline to follow-up using a voxel-level $p < 0.005$. With a liberal voxel-level $p < 0.01$, we observed that more practice time was associated with less longitudinal CBF changes in the junction of occipital, temporal, and cerebellum regions (Supplementary Figure S3). A summary of the two clusters' statistics is listed in Supplementary Table S1. Regional analysis showed that the initially increased CBF gradually reduced with practice time (Supplementary Figure S4). The two subjects with practice time longer than 1000 min exhibited reduced CBF at follow-up, compared to their baseline CBF values. It is worth noting that the region with mixed CBF increase and decrease from different subjects, is very close to the region with longitudinal CBF increases.

3.5. Differences in CBF Functional Connectivity between Baseline and Follow-Up

Significant longitudinal changes in CBF functional connectivity were observed from the baseline to follow-up using a voxel-level $p < 0.005$. Compared to the baseline, we observed significantly increased CBF rsFC between the LMT seed and precuneus area (corrected cluster-level $p = 0.023$) (Figure 2a) and between the RFE seed and the superior frontal area (corrected cluster-level $p < 0.001$) (Figure 2b) and decreased CBF rsFC between the LMT and the temporal area (corrected cluster-level $p = 0.012$) (Figure 2c) at follow-up. A summary of the clusters' statistics is reported in Table 2. Regional analysis showed the rsFC change from the baseline to follow-up with different seeds (Figure 3).

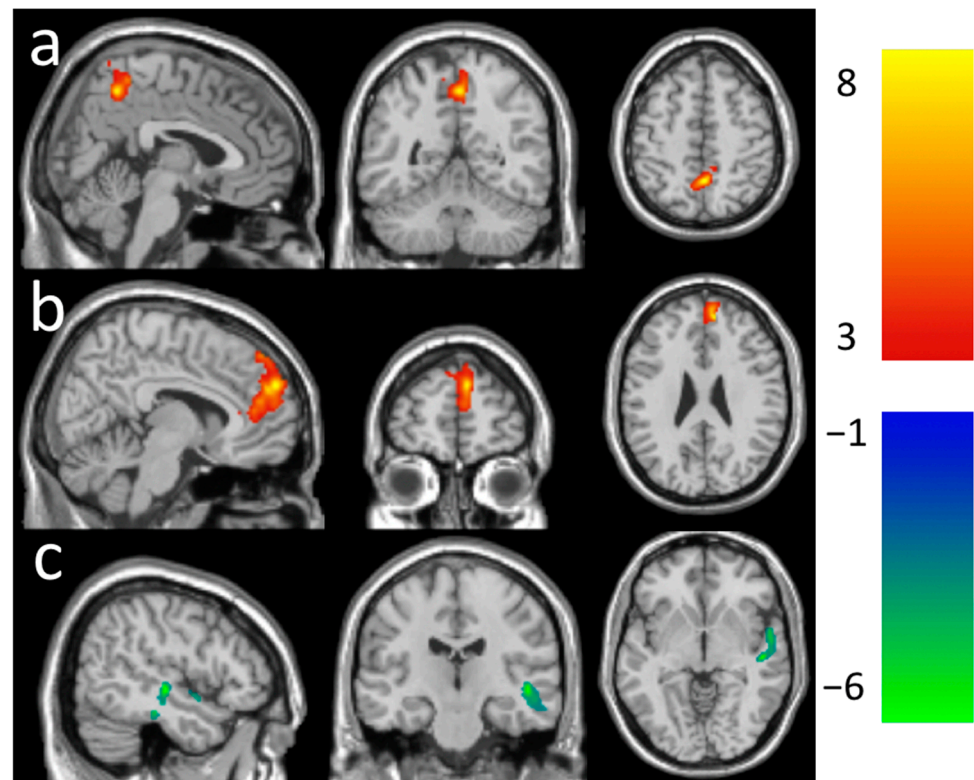


Figure 2. Increased functional connectivity (a) in the precuneus area (peak-T at 4, −52, 52) with the left visual region seed ROI (LMT) and (b) in the frontal region (peak-T at (10, 26, 46)) with the right frontal eye field seed ROI (RFE). (c) Decreased functional connectivity in the superior temporal area (peak-T at (50, −20, −6)) with the left visual region seed ROI (LMT) after 2-month meditation practice at the thresholds of a voxel-level p -value of 0.005 and corrected cluster-level p -value of 0.05. The color bar shows the range of t -values.

Table 2. Summary of cluster-level statistics for clusters showing significant longitudinal rsFC changes between the baseline and the follow-up.

	N Voxels	Local Zscore	Peak-t MNI Coordinates	Mean Beta \pm Std.	Anatomical Locations	% Cluster	% Region
Increased LMT rsFC (Figure 2a)	440	4.14	4, −52, 52	0.25 \pm 0.03	Parietal Lobe		
					Precuneus_R	60.68	8.18
					Precuneus_L	34.77	4.34
					Paracentral_Lobule_R	2.73	1.44
					Limbic System		
Cingulum_Mid_R	1.82	0.36					

Table 2. Cont.

	N Voxels	Local Zscore	Peak-t MNI Coordinates	Mean Beta \pm Std.	Anatomical Locations	% Cluster	% Region
Increased RFE rsFC (Figure 2b)	1038	4.36	10, 50, 26	0.22 ± 0.04	Frontal Lobe		
					Frontal_Sup_Medial_R	49.52	24.09
					Frontal_Sup_Medial_L	19.46	6.75
					Frontal_Sup_L	5.01	1.44
					Frontal_Sup_R	4.72	1.21
					Limbic System		
					Cingulum_Ant_R	20.81	16.45
Decreased LMT rsFC (Figure 2c)	499	3.82	50, -20, -6	-0.23 ± 0.04	Temporal Lobe		
					Temporal_Sup_R	48.30	7.67
					Temporal_Mid_R	24.65	2.79
					Temporal_Inf_R	16.63	2.33
					Temporal_Pole_Sup_R	6.81	2.54
					Heschl_R	2.00	4.02
					Temporal_Pole_Mid_R	1.00	0.42

MNI = Montreal Neurological Institute.

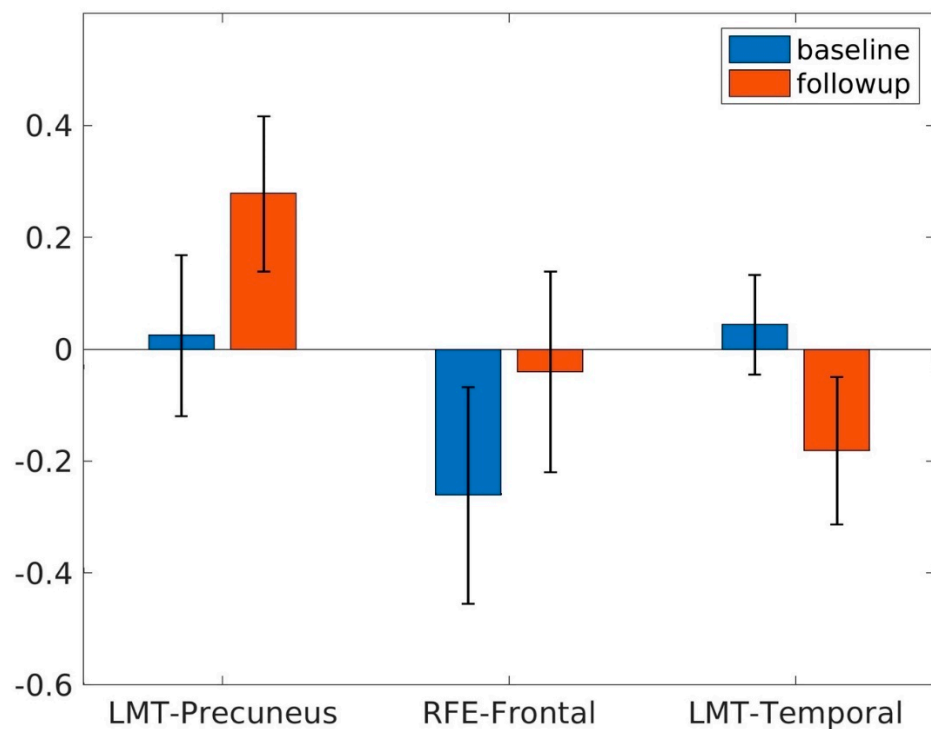


Figure 3. Functional connectivity between the LMT and precuneus, RFE and frontal, and LMT and temporal regions at baseline and follow-up.

3.6. Association of CBF Functional Connectivity with Meditation Practice Time

Longitudinal changes in CBF functional connectivity with the DMN seeds were found to correlate with meditation practice time using a voxel-level $p < 0.005$. After adjusting for the gender effect, the practice time was positively associated with the longitudinal changes in rsFC between the PCC seed and the insular and prefrontal areas (Figure 4a), between the vmPFC seed and the frontal and temporal region (Figure 4c), but negatively associated with the longitudinal changes in rsFC between the PCC seed and the precuneus area (Figure 4b) and between the vmPFC seed and the frontal and parietal area (Figure 4d). A summary of the clusters' statistics is reported in Table 3.

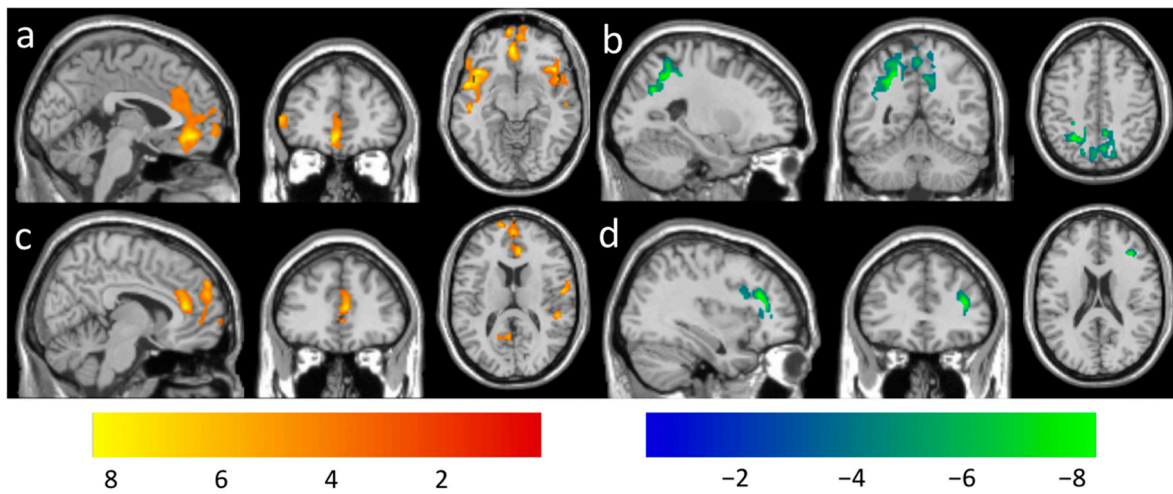


Figure 4. Regions overlaid on a standard brain template in which the meditation practice time was positively associated with functional connectivity with a seed ROI at the (a) PCC (peak-T $-54, 4, -10$), (c) vmPFC (peak-T $8, 36, 14$) and negatively associated with functional connectivity with a seed ROI at the (b) PCC (peak-T $-26, -52, 42$), (d) vmPFC (peak-T $36, 34, 18$) at the thresholds of a voxel-level p -value of 0.005 and corrected cluster-level p -value of 0.05. The color bar shows the range of t -values.

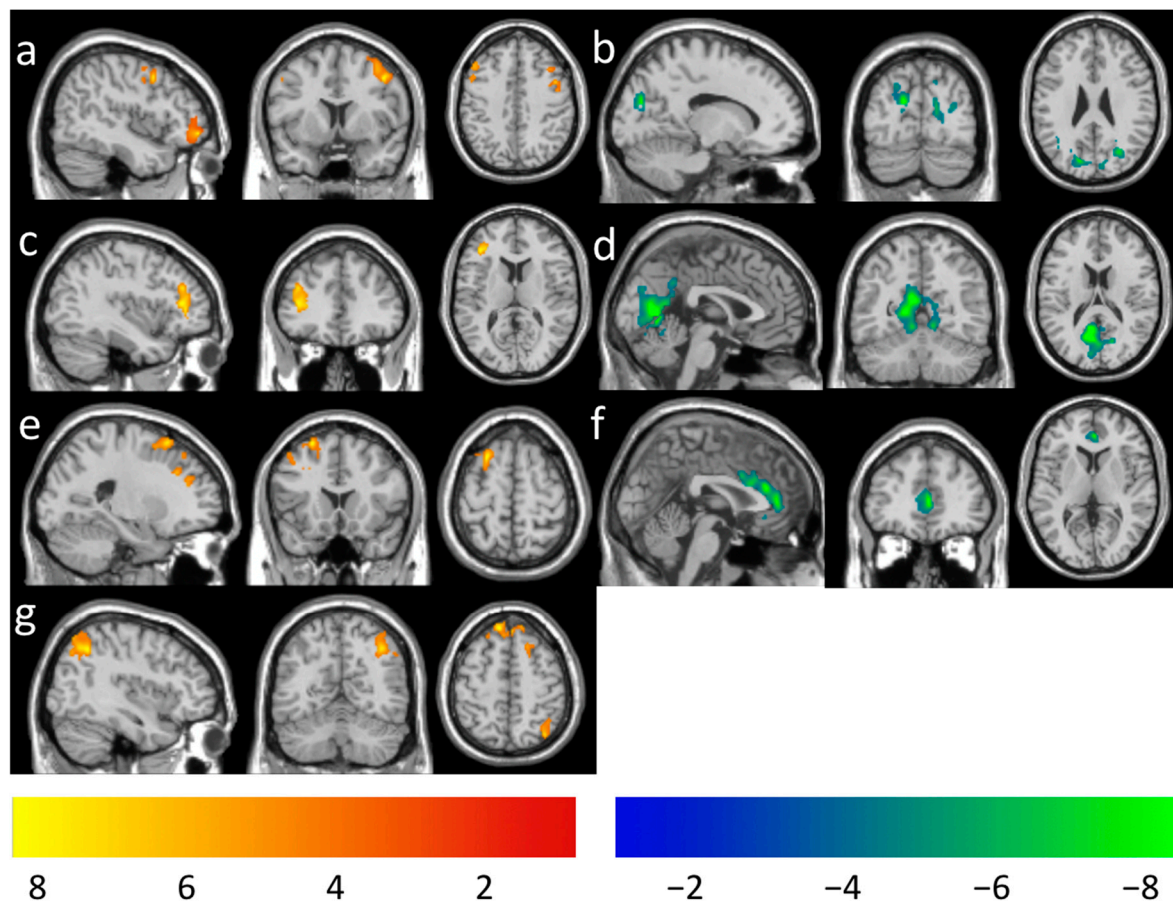


Figure 5. Regions overlaid on a standard brain template in which the meditation practice time was positively associated with functional connectivity with a seed ROI at the (a) RMT (peak-T $44, 8, 44$), (c) LSPL (peak-T $-38, 34, 12$), and (e) RFE (peak-T $24, 18, 60$), (g) LFE (peak-T $40, -56, 46$) and negatively associated with functional connectivity with a seed ROI at the (b) RMT (peak-T $8, -68, 22$), (d) LSPL (peak-T $-2, -64, 4$), and (f) RFE (peak-T $0, 32, 24$) at the thresholds of a voxel-level p -value of 0.005 and corrected cluster-level p -value of 0.05. The color bar shows the range of t -values.

Table 3. Summary of cluster-level statistics for clusters showing significant longitudinal FC changes associated with meditation practice time.

Association with Practice Time	N Voxels	Local Zscore	Peak-t MNI Coordinates	Mean Beta \pm Std. ($\times 10^{-4}$) (/minute)	Anatomical Locations	% Cluster	% Region									
Positive for PCC rsFC (Figure 4a)	2162	4.45	−54, 4, −10	6.45 \pm 1.45	Insula	22.48	26.16									
					Insula_L											
					Temporal Lobe											
					Temporal_Pole_Sup_L			17.44	29.34							
					Temporal_Sup_L			15.17	14.29							
					Temporal_Mid_L			5.18	2.17							
					Heschl_L			2.78	26.67							
					Frontal Lobe											
					Frontal_Inf_Tri_L			14.52	12.42							
					Frontal_Inf_Orb_L			11.05	14.14							
					Frontal_Inf_Oper_L			5.64	11.75							
					Rolandic_Oper_L			3.42	7.47							
					Frontal_Mid_L			1.16	0.51							
								1720	4.10	−4, −42, −12	7.14 \pm 1.28	Limbic System	23.95	29.43		
Cingulum_Ant_L																
Cingulum_Mid_L	3.84	3.40														
Cingulum_Ant_R	2.33	3.05														
Frontal Lobe																
Frontal_Sup_Medial_L	17.44	10.03														
Frontal_Med_Orb_R	15.93	32.01														
Frontal_Med_Orb_L	15.81	37.83														
Rectus_L	6.63	13.38														
Frontal_Sup_Medial_R	6.63	5.34														
Rectus_R	4.59	10.60														
Frontal_Sup_L	2.21	1.06														
	897	4.12	44, 22, −10	5.86 \pm 1.32		Insula	34.23					17.34				
						Insula_R										
					Temporal Lobe											
					Temporal_Pole_Sup_R	24.64		16.52								
					Temporal_Pole_Mid_R	4.91		3.71								
					Temporal_Mid_R	1.67		0.34								
					Frontal Lobe											
					Frontal_Inf_Orb_R	16.50		8.67								
					Frontal_Inf_Oper_R	13.60		8.72								
					Frontal_Inf_Tri_R	3.68		1.53								
						395		3.70	44, −24, 18	5.11 \pm 0.86	Temporal Lobe		42.53	5.35		
											Temporal_Sup_R					
											Heschl_R				14.68	23.29
											Temporal_Mid_R				1.52	0.14
Frontal Lobe																
Rolandic_Oper_R	30.13	8.94														
Insula																
Insula_R	11.14	2.49														

Table 3. Cont.

Association with Practice Time	N Voxels	Local Zscore	Peak-t MNI Coordinates	Mean Beta \pm Std. ($\times 10^{-4}$) (/minute)	Anatomical Locations	% Cluster	% Region
Negative for PCC rsFC (Figure 4b)	2892	5.38	−26, −52, 42	−6.22 \pm 1.38	Parietal Lobe		
					Precuneus_L	26.38	21.63
					Precuneus_R	26.00	23.03
					Parietal_Sup_L	8.78	12.30
					Parietal_Inf_L	6.40	7.56
					Angular_L	3.63	8.95
					Parietal_Sup_R	3.56	4.64
					Postcentral_L	1.28	0.95
					Occipital Lobe		
					Occipital_Mid_R	11.45	15.78
					Occipital_Sup_R	4.88	9.98
					Occipital_Mid_L	3.67	3.24
					Occipital_Sup_L	1.38	2.93
					Cuneus_R	1.35	2.74
					Positive with vmPFC rsFC (Figure 4c)	1108	4.14
Frontal_Sup_Medial_R	33.39	17.34					
Frontal_Sup_Medial_L	27.71	10.26					
Frontal_Sup_L	3.79	1.17					
Limbic System							
Cingulum_Ant_R	27.8	23.46					
Cingulum_Ant_L	5.42	4.29					
Cingulum_Mid_R	1.17	0.59					
	916	3.94	44, −26, 2	5.76 \pm 1.03	Temporal Lobe		
					Temporal_Sup_R	61.68	17.99
					Temporal_Mid_R	9.28	1.93
					Temporal_Inf_R	5.02	1.29
					Heschl_R	2.84	10.44
					Frontal Lobe		
					Rolandic_Oper_R	11.90	8.19
					Precentral_R	1.20	0.33
					Parietal Lobe		
					Postcentral_R	8.08	1.94
						381	3.18
Precuneus_L	45.14	4.88					
Precuneus_R	8.14	0.95					
Occipital Lobe							
Calcarine_L	20.73	3.50					
Cuneus_L	9.71	2.42					
Lingual_L	1.84	0.33					
Limbic System							
Cingulum_Post_L	11.02	9.07					
Cingulum_Mid_R	1.84	0.32					
Cingulum_Post_R	1.57	1.79					
Negative for vmPFC rsFC (Figure 4d)	377	5.16	36, 34, 18	−6.13 \pm 1.31	Frontal Lobe		
					Frontal_Inf_Tri_R	42.18	7.39
					Frontal_Mid_R	27.06	2.00
					Frontal_Inf_Oper_R	23.08	6.22
					Insula		
Insula_R	7.69	1.64					

Table 3. Cont.

Association with Practice Time	N Voxels	Local Zscore	Peak-t MNI Coordinates	Mean Beta \pm Std. ($\times 10^{-4}$) (/minute)	Anatomical Locations	% Cluster	% Region
	361	3.96	22, -68, 52	4.62 \pm 0.86	Parietal Lobe Parietal_Sup_R Angular_R Postcentral_R	72.85 4.99 1.94	11.84 1.03 0.18
					Occipital Lobe Occipital_Sup_R Occipital_Mid_R	17.73 2.22	4.53 0.38
Positive for RMT rsFC (Figure 5a)	596	3.78	44, 8, 44	5.79 \pm 1.13	Frontal Lobe Frontal_Mid_R Precentral_R Frontal_Sup_R	62.58 26.01 11.41	7.31 4.58 1.68
	484	3.76	-50, 28, 28	6.33 \pm 0.98	Frontal Lobe Frontal_Inf_Tri_L Frontal_Mid_L Frontal_Inf_Oper_L Precentral_L	47.73 40.91 7.23 4.13	9.13 4.06 3.37 0.57
	330	4.34	46, 50, -8	5.69 \pm 1.25	Frontal Lobe Frontal_Inf_Orb_R Frontal_Mid_R Frontal_Mid_Orb_R Frontal_Inf_Tri_R Frontal_Sup_R	36.36 28.28 20.61 8.48 6.36	7.03 1.82 6.70 1.30 0.52
Negative for RMT rsFC (Figure 5b)	724	3.89	28, -68, 22	-6.75 \pm 1.40	Parietal Lobe Precuneus_R Parietal_Sup_R	23.07 8.29	5.11 2.70
					Occipital Lobe Occipital_Mid_R Calcarine_R Occipital_Sup_R Cuneus_R	21.41 16.44 15.88 14.92	7.39 6.39 8.14 7.58
	571	4.29	-14, -78, 24	-6.59 \pm 1.10	Occipital Lobe Occipital_Sup_L Occipital_Mid_L Cuneus_L Calcarine_L Parietal Lobe Angular_L Parietal_Sup_L Temporal Lobe Temporal_Mid_L	40.98 22.94 11.38 3.33 16.99 1.40 2.80	17.13 4.01 4.26 0.84 8.27 0.39 0.32
Positive for LSPL rsFC (Figure 5c)	403	3.47	-38, 34, 12	6.10 \pm 1.26	Frontal Lobe Frontal_Mid_L Frontal_Inf_Tri_L Frontal_Sup_L	52.85 40.94 6.20	4.38 6.52 0.69

Table 3. Cont.

Association with Practice Time	N Voxels	Local Zscore	Peak-t MNI Coordinates	Mean Beta \pm Std. ($\times 10^{-4}$) (/minute)	Anatomical Locations	% Cluster	% Region
Negative for LSPL rsFC (Figure 5d)	3681	5.55	−2, −64, 4	−6.49 \pm 1.35	Occipital Lobe		
					Calcarine_L	24.67	40.21
					Lingual_L	16.25	28.54
					Lingual_R	14.34	22.96
					Calcarine_R	12.85	25.42
					Cuneus_L	7.23	17.43
					Parietal Lobe		
					Precuneus_L	9.05	9.44
					Precuneus_R	1.52	1.72
					Cerebellum		
					Cerebellum_4_5_L	3.15	10.31
					Vermis_4_5	1.98	10.98
					Cerebellum_4_5_R	1.33	5.69
					Vermis_6	1.09	10.78
Limbic System							
Cingulum_Post_L	2.50	19.87					
Positive for RFE rsFC (Figure 5e)	727	4.15	−24, 18, 60	−5.95 \pm 1.29	Frontal Lobe		
					Frontal_mid_L	51.03	7.63
					Frontal_Sup_L	33.70	6.81
					Frontal_Inf_Oper_L	7.57	5.30
					Precentral_L	4.68	0.96
					Frontal_Inf_Tri_L	3.03	0.87
Negative for RFE rsFC (Figure 5f)	1010	4.33	0, 32, 24	5.68 \pm 1.20	Limbic System		
					Cingulum_Ant_L	56.63	40.86
					Cingulum_Mid_L	20.69	10.77
					Cingulum_Ant_R	25.54	11.96
					Cingulum_Mid_R	2.28	1.04
					Frontal Lobe		
					Frontal_sup_Medial_L	4.16	1.40
Positive for LFE rsFC (Figure 5g)	546	3.92	40, −56, 46	5.84 \pm 1.26	Parietal Lobe		
					Angular_R	70.51	21.97
					Parietal_Inf_R	17.40	7.06
					Parietal_Sup_R	10.99	2.70
	543	4.39	26, 20, 64	5.26 \pm 0.88	Frontal Lobe		
					Frontal_Sup_R	46.04	6.16
					Frontal_Sup_Medial_L	23.39	4.24
					Frontal_Sup_Medial_R	25.65	3.98
					Frontal_Sup_L	11.42	1.72
					Supp_Motor_Area_R	1.66	0.38
Frontal_Mid_L	1.66	0.19					

MNI = Montreal Neurological Institute.

Longitudinal changes in CBF functional connectivity with the DAN seeds were found to correlate with meditation practice time using a voxel-level $p < 0.005$. After adjusting for the gender effect, the practice time was found to be positively associated with the longitudinal changes in rsFC between the RMT seed and the middle/inferior frontal area (Figure 5a), between the LSPL seed and the middle/inferior frontal area (Figure 5c), between the RFE seed and the superior/middle frontal area (Figure 5e), and between the LFE seed and the frontal and angular/parietal area (Figure 5g). The meditation practice time was found to be negatively associated with the longitudinal changes in rsFC between the RMT seed and the occipitoparietal area (Figure 5b), between the LSPL seed and the occipitoparietal area (Figure 5d), and between the RFE seed and the anterior/middle

cingulate area (Figure 5f). A summary of the clusters' statistics is also reported in Table 3. Post hoc regional analysis showed that the longitudinal changes of rsFC may change from a positive to a negative direction (increased rsFC to decreased rsFC at follow-up compared to the baseline) (Supplementary Figure S5a,c,e) or from negative to positive (decreased rsFC to increased rsFC at follow-up, compared to the baseline) (Supplementary Figure S5b,d,f) as more meditation practice time was involved. We also noticed that the switching time between different polarities is about 500 to 700 min of meditation practice time. A complete summary of post hoc regional correlation with total meditation practice time is listed in Supplementary Table S2.

4. Discussion

In this longitudinal study, altered rsFC were found following 2-month meditation practice using the dASL technique. The LMT rsFC significantly increased in the precuneus region but decreased in the superior temporal region; the RFE rsFC significantly increased in the superior frontal region. Total meditation practice time was positively associated with rsFC between PCC and insular/temporal/mPFC, vmPFC and frontal/temporal/precuneus, RMT and middle/inferior frontal, LSPL/RSPL and left middle/inferior frontal, RFE and superior/middle frontal, LFE and frontal and angular/parietal regions. Total meditation practice time was negatively associated with rsFC between PCC and precuneus/occipital, vmPFC and frontal and parietal, RMT and occipitoparietal, LSPL and left occipitoparietal, and RFE and anterior/middle cingulate regions.

The longitudinal increase in rsFC between the LMT and precuneus and between RFE and superior frontal regions expands the current literature that reports the stronger rsFC between certain regions of the DMN and certain regions of the DAN [33,45]. These results are also consistent with the enhanced DMN-DAN rsFC using the BOLD fMRI technique and advanced denoising technique. The strengthened DMN-DAN rsFC suggests greater synergy coherence between self-referential and attention and may facilitate switching between the networks [46]. The enhanced coupling of DMN and DAN may reflect the benefits of meditation processes, such as improved attention regulation and self-monitoring.

Longer meditation practice time was associated with (1) increased PCC-rsFC and vmPFC-rsFC with the mPFC/ACC area and (2) increased PCC-rsFC with the insula area. These results extend the prior cross-sectional study that showed greater DMN-rsFC with the mPFC region [34] and PCC-rsFC with the ACC region [33] in experienced meditators than healthy controls. Cross-sectional studies also reported the increased mPFC-rsFC with the insula region in experienced meditators compared to controls [33,45] and increased salience network rsFC with the PCC region [47] in the high practice group, compared to the low practice group. Insula, which is the core region of the brain salience network, is thought to detect salient features for additional processing and act as a switchboard to direct other brain networks [48–50]. The direct causal influence of the insular cortex on PCC activity has been established [50], which provides further mechanistic evidence of the salience network exerting influence on DMN through meditation.

Meditation practice time was associated with increased dorsal lateral prefrontal cortex (DLPFC) rsFC with almost all the DAN seeds, including RMT, LSPL/RSPL, LFE/RFE. The DLPFC region, a key region in the frontoparietal control network (FPN), serves to initiate and regulate attention and cognitive control in response to salient stimuli [31,32]. Our results are in good accordance with the work by Taren et al. that showed mindfulness training increases rsFC between DLPFC and DAN (although they used the DLPFC as a seed for rsFC investigation) [51] and by Froeliger et al. that showed increased rsFC between FPN and DAN (specifically between DLPFC and inferior parietal regions) [30]. Consistent with its anatomical connections [32,52], the DLPFC region extends its rsFC to all DAN regions, instead of prior reported specific regions, indicating the higher sensitivity of our technique on rsFC. The increased rsFC between DLPFC and all DAN seeds suggests that FAM can enhance the top-down control ability for attention selection in the functionally connected DAN system. In addition, we have extended the correlation of practice time

with DAN-FPN rsFC at a single time point [30] to the correlation with the changes of DAN-FPN rsFC. These longitudinal results demonstrated that the changes of DAN-FPN rsFC are caused by meditation practice.

Meditation practice time was associated with decreased vmPFC-rsFC with DLPFC. These findings are consistent with reduced rsFC between DMN and FPN/CEN for meditators [53,54]. Conversely, a recent study reported a positive correlation between meditation experience and mPFC-CEN rsFC [55], which seems to contradict our increased anticorrelation with practice time (Supplementary Figure S5c). However, their further analysis resolved the conflicts by noticing that the intermediate meditators (<1130 h of practice, approximately three years of 1 h daily practice) exhibited significant increases in anticorrelations between CEN and MPFC, whereas more experienced meditators (>1130 h of practice) have the anticorrelations returned to a premeditation state. Our longitudinal results, together with the cross-sectional results, further underscore that meditation changes brain connectivity in a nonlinear way. The increased anticorrelations between CEN and DMN suggest that CEN negatively regulates DMN (i.e., suppresses the brain activity of DMN), and thereby meditators probably spend less time in a mind-wandering state during daily life [56].

Meditation practice time was associated with decreased RMT-rsFC or LSPL/RSPL-rsFC with visual/occipital regions. These results are in line with lower meditative-state connectivity between attention and visual networks in more experienced meditators [47]. These results suggest that meditators may have a more efficient attentional allocation, with decreased attentional resources being devoted to the visual processing domain. In addition, we also observed a negative association between meditation practice time and RFE-ACC rsFC. ACC is anatomically connected with the frontal eye fields and assigns appropriate control to visual attention [57]. The reduced rsFC between ACC and RFE also indicates meditation exerting more efficient attentional control, with a decreased assignment to visual attention.

We found a significant negative correlation between PCC-precuneus/inferior parietal connectivity and meditation practice time. These results were a little surprising to us because we observed a positive correlation between PCC-mPFC and mPFC-mPFC connectivity and meditation practice time. However, these results are consistent with the anticorrelation in DMN (between nearby DMN regions: precuneus and inferior parietal regions in their findings) [29]. These findings are also in line with several studies that have found reduced connectivity within certain regions of the DMN in experienced meditators, compared to their novice counterparts [28,54,58].

We observed that the individual differences in meditation practice time were associated with rsFC in markedly more pairs of brain regions using the dASL technique compared with the multi-echo BOLD fMRI technique (results shown as a separate publication [20]) in the same participant sample. Meditation practice time was positively correlated with DMN-DAN rsFC changes using the multi-echo BOLD fMRI technique. By contrast, meditation practice time was positively correlated with DMN-DAN rsFC changes, and also positively correlated DMN-SN and DAN-FPN rsFC changes, and negatively correlated with DMN-FPN rsFC using the dASL technique. The extra rsFC findings using dASL reveal that FPN and SN are involved in brain attentional switching between DMN and DAN, and 2-month meditation practice can enhance the communication between those networks, reflecting the higher sensitivity of the dASL technique in characterizing the rsFC. We postulate that the higher sensitivity of dASL is because its signals are more robust to physiological noises and small motion artifacts via the incorporation of strong background suppression techniques. Strong background suppression has been proven useful in limiting physiological noises and motion-induced subtraction errors in renal ASL applications [59,60]. Meanwhile, we found fewer pairs of brain regions with longitudinal rsFC changes following 2-month meditation practice using the dASL technique. CBF rsFC changes from the baseline to follow-up experienced different polarities (some participants had increased rsFC but others had decreased rsFC from the baseline to follow-up) (see

Supplementary Figure S5). Different polarities in CBF rsFC across subjects in our study cancel each other out, and therefore, significant changes of CBF rsFC on group level were less prominent. We expect that the CBF rsFC using dASL will achieve superior sensitivity in detecting longitudinal changes when all participants have either increased rsFC or decreased rsFC. Increased rsFC or decreased rsFC across participants can be sensitively detected when all participants practice meditation longer than the zero-crossing time (e.g., ~750 min for PFC-parietal rsFC in Supplementary Figure S5c). The polarity differences in longitudinal rsFC changes between dASL and multi-echo BOLD presumably emerge from their different signal sources. dASL signals are from a single source CBF, while BOLD signals reflect a combination of effects from blood oxygenation, cerebral blood volume, CBF, and metabolic rate of oxygen changes [61–64]. BOLD signal fluctuations from sources other than CBF may have contributed to the polarity difference, i.e., different signs of rsFC changes, compared to dASL.

This study has some limitations. First, the study has a small sample size. However, the study was intended to serve as a preliminary study to test the sensitivity of dASL in meditation effects. The observed significant rsFC changes after a 2-month meditation practice with this small sample size support the large effect size from the dASL method. Second, a control group was not included in the study. However, the longitudinal changes of rsFC were related to meditation practice time, suggesting that the rsFC changes emerge from meditation practice itself, not from expectancy bias. Third, a short follow-up period and only one follow-up time were used in the study. Therefore, the results may not be generalized to the effect of long-term meditation. Further investigation with a larger sample size, matched control group and longer follow-up is warranted to validate the effect of meditation practice time on brain rsFC changes.

5. Conclusions

Our significant findings using dASL support further investigation into the power of the technique in meditation studies. Two-month meditation is associated with the changes of rsFC and the changes of rsFC are associated with practice time. These findings suggest that the practice of meditation can strengthen the efficient control of FPN on fast switching between DMN and DAN and improve the utilization of attentional resources with reduced focus on visual processing.

Supplementary Materials: The following are available online at <https://www.mdpi.com/article/10.3390/brainsci11101263/s1>, Figure S1, Representative dASL images from the inferior to superior slice (column 1 to 5) at four time points (row 1 to 4) and temporal SNR across all time points (row 5). The scale bars are shown on the right. Figure S2, Regions overlaid on a standard brain template in which (a) follow-up CBF > baseline CBF, (b) follow-up CBF < baseline CBF at the thresholds of a voxel-level p -value of 0.01 and corrected cluster-level p -value of 0.05. The color bar shows the range of t -values; Figure S3, Regions overlaid on a standard brain template in which the meditation practice time was negatively associated with CBF changes at the threshold of a voxel-level p -value of 0.01 and corrected cluster-level p -value of 0.05. Color bar shows the range of t -values; Figure S4, Meditation practice time was negatively associated with relative CBF in the junction of occipital, temporal, and cerebellum regions ($r = -0.89$, $p = 0.0013$); Figure S5, Post-hoc regional analysis confirms that the association of meditation practice time with longitudinal changes of (a) PCC-parietal rsFC, (b) PCC-insula rsFC, (c) PFC-parietal rsFC, (d) PFC-frontal rsFC, (e) LSPL-occipital rsFC, and (f) LSPL-frontal rsFC. The association between longitudinal changes of rsFC and meditation practice time appears not driven by outliers; Table S1. Summary of cluster-level statistics for clusters showing significant longitudinal CBF changes from the base-line to the follow-up; Table S2. Summary of Post-hoc regional analysis results on the association between rsFC changes and practice time.

Author Contributions: Z.Z., W.-M.L. and W.D. (Weiyang Dai) conceived and designed the experiments. Z.Z., T.D.Z. and W.D. (Wenna Duan) performed the experiments and analyzed the data. Z.Z. and W.D. (Weiyang Dai) wrote the paper. W.-M.L., W.D. (Wenna Duan), T.D.Z., L.Z., G.W. and A.K.A. contributed to the discussion and revised the manuscript. All authors have read and agreed to the published version of the manuscript.

Funding: This research was funded by the National Institute on Aging, grant number R01AG066430 Alzheimer's Association, grant number AARF-18-566347; and Binghamton University, Transdisciplinary Areas of Excellence (TAE) seed grant number 1154428 and the APC was funded by R01AG066430, AARF-18-566347, and 1154428.

Institutional Review Board Statement: The study was conducted according to the guidelines of the Declaration of Helsinki, and approved by the Institutional Review Board (or Ethics Committee) of Cornell University (protocol code 1608006527 and date of approval 8 September 2017).

Informed Consent Statement: Informed consent was obtained from all subjects involved in the study.

Data Availability Statement: Raw data were generated from the MRI scanner. Reconstruction software is the vendor's proprietary product. Sharing of derived data will be supported by direct request. After publishing our main findings, requests for data will be evaluated on a case-by-case basis. Before sharing data, we will make sure that all data are free of identifiers that could directly or indirectly link information to an individual and that all sharing is compliant with institutional and IRB policies.

Acknowledgments: T. D. Zhou, affiliated with Vestal High School, Vestal, NY, USA, conducted his research in the Department of Computer Science at Binghamton University when he was a visiting research assistant in Weiyang Dai's research group.

Conflicts of Interest: None of the authors has a conflict of interest to disclose.

Abbreviations

automated anatomical labeling (AAL); anterior cingulate cortex (ACC); blood-oxygen-level dependent (BOLD); cerebral blood flow (CBF); default mode network (DMN); dorsal attention network (DAN); dorsal lateral prefrontal cortex (DLPFC); dynamic arterial spin labeling (dASL); echo time (TE); family wise error (FWE); fast spin echo (FSE); field of view (FOV); focused attention meditation (FAM); frontoparietal control network (FPN); functional connectivity (FC); general linear model (GLM); gray matter (GM); inversion time (TI); left frontal eye field (LFE); left medial temporal (LMT); left superior parietal lobule (LSPL); magnetization prepared rapid gradient echo (MPRAGE); orbitofrontal cortex (OFC); posterior cingulate cortex (PCC); post-traumatic stress disorder (PTSD); pseudo-continuous arterial spin labeling (PCASL); receiver bandwidth (rBW); repetition time (TR); resting-state functional connectivity (rsFC); right frontal eye (RFE); right middle temporal area (RMT); right superior parietal lobule (RSPL); regions of interest (ROIs); structural magnetic resonance imaging (sMRI); salience network (SN); signal-to-noise ratio (SNR); ventromedial prefrontal cortex (vmPFC).

References

1. Prakash, R.S.; Whitmoyer, P.; Aldao, A.; Schirda, B. Mindfulness and emotion regulation in older and young adults. *Aging Ment. Health* **2015**, *21*, 77–87. [[CrossRef](#)]
2. Hölzel, B.K.; Lazar, S.W.; Gard, T.; Schuman-Olivier, Z.; Vago, D.R.; Ott, U. How does mindfulness meditation work? Proposing mechanisms of action from a conceptual and neural perspective. *Perspect. Psychol. Sci.* **2011**, *6*, 537–559. [[CrossRef](#)]
3. Zeidan, F.; Johnson, S.K.; Diamond, B.J.; David, Z.; Goolkasian, P. Mindfulness meditation improves cognition: Evidence of brief mental training. *Conscious. Cogn.* **2010**, *19*, 597–605. [[CrossRef](#)]
4. Moore, A.; Gruber, T.; Derose, J.; Malinowski, P. Regular, brief mindfulness meditation practice improves elec-trophysiological markers of attentional control. *Front. Hum. Neurosci.* **2012**, *6*, 18. [[CrossRef](#)]
5. Banks, J.B.; Welhaf, M.S.; Srour, A. The protective effects of brief mindfulness meditation training. *Conscious. Cogn.* **2015**, *33*, 277–285. [[CrossRef](#)]
6. Chien, W.T.; Thompson, D. Effects of a mindfulness-based psychoeducation programme for Chinese patients with schizophrenia: 2-year follow-up. *Br. J. Psychiatry* **2014**, *205*, 52–59. [[CrossRef](#)] [[PubMed](#)]
7. Yang, C.-C.; Barrós-Loscertales, A.; Pinazo, D.; Ventura-Campos, N.; Borchardt, V.; Bustamante, J.-C.; Rodríguez-Pujadas, A.; Fuentes-Claramonte, P.; Balaguer, R.; Avila, C.; et al. State and training effects of mindfulness meditation on brain networks reflect neuronal mechanisms of its antidepressant effect. *Neural Plast.* **2016**, *2016*, 9504642. [[CrossRef](#)] [[PubMed](#)]
8. Ludwig, D.S.; Kabat-Zinn, J. Mindfulness in medicine. *JAMA* **2008**, *300*, 1350–1352. [[CrossRef](#)]

9. Janssen, L.; Kan, C.C.; Carpentier, P.J.; Sizoo, B.; Hepark, S.; Grutters, J.; Donders, R.; Buitelaar, J.K.; Speckens, A.E. Mindfulness based cognitive therapy versus treatment as usual in adults with attention deficit hyperactivity disorder (ADHD). *BMC Psychiatry* **2015**, *15*, 216. [[CrossRef](#)] [[PubMed](#)]
10. Hölzel, B.K.; Ott, U.; Gard, T.; Hempel, H.; Weygandt, M.; Morgen, K.; Vaitl, D. Investigation of mindfulness meditation practitioners with voxel-based morphometry. *Soc. Cogn. Affect. Neurosci.* **2007**, *3*, 55–61. [[CrossRef](#)]
11. Vestergaard-Poulsen, P.; van Beek, M.; Skewes, J.; Bjarkam, C.R.; Stubberup, M.; Bertelsen, J.; Roepstorff, A. Long-term meditation is associated with increased gray matter density in the brain stem. *Neuroreport* **2009**, *20*, 170–174. [[CrossRef](#)] [[PubMed](#)]
12. Hernández, S.E.; Suero, J.; Barros, A.; González-Mora, J.L.; Rubia, K. Increased Grey Matter Associated with Long-Term Sahaja Yoga Meditation: A Voxel-Based Morphometry Study. *PLoS ONE* **2016**, *11*, e0150757. [[CrossRef](#)] [[PubMed](#)]
13. Grant, J.A.; Duerden, E.G.; Courtemanche, J.; Cherkasova, M.; Duncan, G.H.; Rainville, P. Cortical thickness, mental absorption and meditative practice: Possible implications for disorders of attention. *Biol. Psychol.* **2013**, *92*, 275–281. [[CrossRef](#)] [[PubMed](#)]
14. Grant, J.A.; Courtemanche, J.; Duerden, E.G.; Duncan, G.H.; Rainville, P. Cortical thickness and pain sensitivity in zen meditators. *Emotion* **2010**, *10*, 43–53. [[CrossRef](#)]
15. Yang, C.C.; Barros-Loscertales, A.; Li, M.; Pinazo, D.; Borchardt, V.; Avila, C.; Walter, M. Alterations in brain structure and amplitude of low-frequency after 8 weeks of mindfulness meditation training in meditation naive subjects. *Sci. Rep.* **2019**, *9*, 10977. [[CrossRef](#)] [[PubMed](#)]
16. Lazar, S.W.; Kerr, C.E.; Wasserman, R.H.; Gray, J.R.; Greve, D.N.; Treadway, M.T.; McGarvey, M.; Quinn, B.T.; Dusek, J.A.; Benson, H.; et al. Meditation experience is associated with increased cortical thickness. *Neuroreport* **2005**, *16*, 1893–1897. [[CrossRef](#)]
17. Holzel, B.K.; Carmody, J.; Evans, K.C.; Hoge, E.A.; Dusek, J.A.; Morgan, L.; Pitman, R.K.; Lazar, S.W. Stress reduction correlates with structural changes in the amygdala. *Soc. Cogn. Affect. Neurosci.* **2010**, *5*, 11–17. [[CrossRef](#)] [[PubMed](#)]
18. Holzel, B.K.; Carmody, J.; Vangel, M.; Congleton, C.; Yerramsetti, S.M.; Gard, T.; Lazar, S.W. Mindfulness practice leads to increases in regional brain gray matter density. *Psychiatry Res.* **2011**, *191*, 36–43. [[CrossRef](#)]
19. Vincent, J.L.; Kahn, I.; Snyder, A.Z.; Raichle, M.E.; Buckner, R.L. Evidence for a frontoparietal control system revealed by intrinsic functional connectivity. *J. Neurophysiol.* **2008**, *100*, 3328–3342. [[CrossRef](#)]
20. Zhang, Z.; Luh, W.-M.; Duan, W.; Zhou, G.D.; Weinschenk, G.; Anderson, A.K.; Dai, W. Longitudinal effects of meditation on brain resting-state functional connectivity. *Sci. Rep.* **2021**, *11*, 11361. [[CrossRef](#)]
21. Biswal, B.; Yetkin, F.Z.; Haughton, V.M.; Hyde, J.S. Functional connectivity in the motor cortex of resting human brain using echoplanar MRI. *Magn. Reson. Med.* **1995**, *34*, 537–541. [[CrossRef](#)]
22. Mooneyham, B.W.; Mrazek, M.D.; Mrazek, A.J.; Schooler, J.W. Signal or noise: Brain network interactions underlying the experience and training of mindfulness. *Ann. N. Y. Acad. Sci.* **2016**, *1369*, 240–256. [[CrossRef](#)]
23. Dai, W.; Garcia, D.; de Bazelaire, C.; Alsop, D.C. Continuous flow-driven inversion for arterial spin labeling using pulsed radio frequency and gradient fields. *Magn. Reson. Med.* **2008**, *60*, 1488–1497. [[CrossRef](#)]
24. Dai, W.; Varma, G.; Scheidegger, R.; Alsop, D.C. Quantifying fluctuations of resting state networks using arterial spin labeling perfusion MRI. *J. Cereb. Blood Flow Metab.* **2016**, *36*, 463–473. [[CrossRef](#)]
25. Birn, R.M.; Murphy, K.; Bandettini, P.A. The effect of respiration variations on independent component analysis results of resting state functional connectivity. *Hum. Brain Mapp.* **2008**, *29*, 740–750. [[CrossRef](#)] [[PubMed](#)]
26. Power, J.D.; Barnes, K.A.; Snyder, A.Z.; Schlaggar, B.L.; Petersen, S.E. Spurious but systematic correlations in functional connectivity MRI networks arise from subject motion. *Neuroimage* **2012**, *59*, 2142–2154. [[CrossRef](#)] [[PubMed](#)]
27. Hamame, C.M.; Vidal, J.R.; Ossandon, T.; Jerbi, K.; Dalal, S.S.; Minotti, L.; Bertrand, O.; Kahane, P.; Lachaux, J.P. Reading the mind's eye: Online detection of visuo-spatial working memory and visual imagery in the inferior temporal lobe. *Neuroimage* **2012**, *59*, 872–879. [[CrossRef](#)] [[PubMed](#)]
28. Taylor, V.A.; Grant, J.; Daneault, V.; Scavone, G.; Breton, E.; Roffe-Vidal, S.; Courtemanche, J.; Lavarenne, A.S.; Beaugregard, M. Impact of mindfulness on the neural responses to emotional pictures in experienced and beginner meditators. *Neuroimage* **2011**, *57*, 1524–1533. [[CrossRef](#)]
29. Berkovich-Ohana, A.; Harel, M.; Hahamy, A.; Arieli, A.; Malach, R. Alterations in task-induced activity and resting-state fluctuations in visual and DMN areas revealed in long-term meditators. *Neuroimage* **2016**, *135*, 125–134. [[CrossRef](#)]
30. Froeliger, B.; Garland, E.L.; Kozink, R.V.; Modlin, L.A.; Chen, N.-K.; McClernon, F.J.; Greeson, J.M.; Sobin, P. Meditation-state Functional Connectivity (msFC): Strengthening of the dorsal attention network and beyond. *Evid.-Based Complement. Altern. Med.* **2012**, *2012*, 680407. [[CrossRef](#)]
31. Dosenbach, N.U.F.; Fair, D.A.; Miezin, F.M.; Cohen, A.L.; Wenger, K.K.; Dosenbach, R.A.T.; Fox, M.D.; Snyder, A.Z.; Vincent, J.L.; Raichle, M.E.; et al. Distinct brain networks for adaptive and stable task control in humans. *Proc. Natl. Acad. Sci. USA* **2007**, *104*, 11073–11078. [[CrossRef](#)]
32. Goldman-Rakic, P.S. Architecture of the prefrontal cortex and the central executive. *Ann. N. Y. Acad. Sci.* **1995**, *769*, 71–83. [[CrossRef](#)]
33. Brewer, J.A.; Worhunsky, P.D.; Gray, J.R.; Tang, Y.-Y.; Weber, J.; Kober, H. Meditation experience is associated with differences in default mode network activity and connectivity. *Proc. Natl. Acad. Sci. USA* **2011**, *108*, 20254–20259. [[CrossRef](#)] [[PubMed](#)]
34. Jang, J.H.; Jung, W.H.; Kang, D.H.; Byun, M.S.; Kwon, S.J.; Choi, C.H.; Kwon, J.S. Increased default mode network connectivity associated with meditation. *Neurosci. Lett.* **2011**, *487*, 358–362. [[CrossRef](#)]

35. Garrison, K.A.; Scheinost, D.; Constable, R.T.; Brewer, J.A. BOLD signal and functional connectivity associated with loving kindness meditation. *Brain Behav.* **2014**, *4*, 337–347. [[CrossRef](#)] [[PubMed](#)]
36. Jao, T.; Li, C.-W.; Vértes, P.E.; Wu, C.W.; Achard, S.; Hsieh, C.-H.; Liou, C.-H.; Chen, J.-H.; Bullmore, E.T. Large-scale functional brain network reorganization during taoist meditation. *Brain Connect.* **2016**, *6*, 9–24. [[CrossRef](#)]
37. King, A.P.; Block, S.R.; Sripatha, R.K.; Rauch, S.; Giardino, N.; Favorite, T.; Angstadt, M.; Kessler, D.; Welsh, R.; Liberzon, I. Altered Default mode network (Dmn) resting state functional connectivity following a mindfulness based exposure therapy for Posttraumatic stress disorder (Ptsd) in combat veterans of Afghanistan and Iraq. *Depress. Anxiety* **2016**, *33*, 289–299. [[CrossRef](#)] [[PubMed](#)]
38. Zhang, Z.; Duan, W.; Bolo, N.R.; Tamminga, C.; Clementz, B.A.; Pearlson, G.D.; Keshavan, M.; Alsop, D.C.; Dai, W. Sensitivity of dynamic ASL and resting-state bold in patients with bipolar disorder. In Proceedings of the 28th ISMRM, Virtual Conference, 8–14 August 2020; Volume 28, p. 3874.
39. Maleki, N.; Dai, W.; Alsop, D.C. Optimization of background suppression for arterial spin labeling perfusion imaging. *Magn. Reson. Mater. Phys. Biol. Med.* **2012**, *25*, 127–133. [[CrossRef](#)]
40. Zhao, L.; Alsop, D.C.; Detre, J.A.; Dai, W. Global fluctuations of cerebral blood flow indicate a global brain network independent of systemic factors. *J. Cereb. Blood Flow Metab.* **2019**, *39*, 302–312. [[CrossRef](#)] [[PubMed](#)]
41. Alsop, D.; Detre, J.A. Reduced transit-time sensitivity in noninvasive magnetic resonance imaging of human cerebral blood flow. *J. Cereb. Blood Flow Metab.* **1996**, *16*, 1236–1249. [[CrossRef](#)]
42. Wang, J.; Alsop, D.; Li, L.; Listerud, J.; Gonzalez-At, J.B.; Schnall, M.D.; Detre, J.A. Comparison of quantitative perfusion imaging using arterial spin labeling at 1.5 and 4.0 Tesla. *Magn. Reson. Med.* **2002**, *48*, 242–254. [[CrossRef](#)]
43. Buxton, R.B.; Frank, L.R.; Wong, E.C.; Siewert, B.; Warach, S.; Edelman, R.R. A general kinetic model for quantitative perfusion imaging with arterial spin labeling. *Magn. Reson. Med.* **1998**, *40*, 383–396. [[CrossRef](#)] [[PubMed](#)]
44. Lacalle-Aurioles, M.; Aleman-Gomez, Y.; Guzman-De-Villoria, J.A.; Cruz-Orduna, I.; Olazaran, J.; Mateos-Perez, J.M.; Martino, M.E.; Desco, M. Is the cerebellum the optimal reference region for intensity normalization of perfusion MR studies in early Alzheimer’s disease? *PLoS ONE* **2013**, *8*, e81548.
45. Kilpatrick, L.A.; Suyenobu, B.Y.; Smith, S.R.; Bueller, J.A.; Goodman, T.; Creswell, J.D.; Tillisch, K.; Mayer, E.A.; Naliboff, B.D. Impact of mindfulness-based stress reduction training on intrinsic brain connectivity. *Neuroimage* **2011**, *56*, 290–298. [[CrossRef](#)] [[PubMed](#)]
46. Seeley, W.W.; Menon, V.; Schatzberg, A.F.; Keller, J.; Glover, G.H.; Kenna, H.; Reiss, A.L.; Greicius, M.D. Dissociable intrinsic connectivity networks for salience processing and executive control. *J. Neurosci.* **2007**, *27*, 2349–2356. [[CrossRef](#)]
47. Hasenkamp, W.; Barsalou, L.W. Effects of meditation experience on functional connectivity of distributed brain networks. *Front. Hum. Neurosci.* **2012**, *6*, 38. [[CrossRef](#)]
48. Uddin, L. Salience processing and insular cortical function and dysfunction. *Nat. Rev. Neurosci.* **2015**, *16*, 55–61. [[CrossRef](#)]
49. Menon, V.; Uddin, L.Q. Saliency, switching, attention and control: A network model of insula function. *Brain Struct. Funct.* **2010**, *214*, 655–667. [[CrossRef](#)] [[PubMed](#)]
50. Sridharan, D.; Levitin, D.J.; Menon, V. A critical role for the right fronto-insular cortex in switching between central-executive and default-mode networks. *Proc. Natl. Acad. Sci. USA* **2008**, *105*, 12569–12574. [[CrossRef](#)]
51. Taren, A.A.; Gianaros, P.J.; Greco, C.M.; Lindsay, E.; Fairgrieve, A.; Brown, K.W.; Rosen, R.K.; Ferris, J.L.; Julson, E.; Marsland, A.L.; et al. Mindfulness meditation training and executive control network resting state functional connectivity: A randomized controlled trial. *Psychosom. Med.* **2017**, *79*, 674–683. [[CrossRef](#)]
52. He, B.J.; Snyder, A.Z.; Vincent, J.L.; Epstein, A.; Shulman, G.L.; Corbetta, M. Breakdown of functional connectivity in frontoparietal networks underlying behavioral deficits in spatial neglect. *Neuron* **2007**, *53*, 905–918. [[CrossRef](#)]
53. Kemmer, P.B.; Guo, Y.; Wang, Y.; Pagnoni, G. Network-based characterization of brain functional connectivity in Zen practitioners. *Front. Psychol.* **2015**, *6*, 603. [[CrossRef](#)]
54. Doll, A.; Holzel, B.K.; Boucard, C.C.; Wohlschlagel, A.M.; Sorg, C. Mindfulness is associated with intrinsic functional connectivity between default mode and salience networks. *Front. Hum. Neurosci.* **2015**, *9*, 461. [[CrossRef](#)]
55. Bauer, C.C.C.; Whitfield-Gabrieli, S.; Díaz, J.L.; Pasaye, E.H.; Barrios, F.A. From state to trait meditation: Reconfiguration of central executive and default mode networks. *Eneuro* **2019**, *6*. [[CrossRef](#)]
56. Brandmeyer, T.; Delorme, A. Reduced mind wandering in experienced meditators and associated EEG correlates. *Exp. Brain Res.* **2018**, *236*, 2519–2528. [[CrossRef](#)]
57. Posner, M.; DiGirolamo, G. Executive attention: Conflict, target detection, and cognitive control. In *The Attentive Brain*; Parasuraman, R., Ed.; MIT Press: Cambridge, MA, USA, 1988.
58. Hasenkamp, W.; Wilson-Mendenhall, C.D.; Duncan, E.; Barsalou, L.W. Mind wandering and attention during focused meditation: A fine-grained temporal analysis of fluctuating cognitive states. *Neuroimage* **2012**, *59*, 750–760. [[CrossRef](#)] [[PubMed](#)]
59. Robson, P.M.; Madhuranthakam, A.J.; Dai, W.; Pedrosa, I.; Rofsky, N.M.; Alsop, D. Strategies for reducing respiratory motion artifacts in renal perfusion imaging with arterial spin labeling. *Magn. Reson. Med.* **2009**, *61*, 1374–1387. [[CrossRef](#)] [[PubMed](#)]
60. Taso, M.; Guidon, A.; Alsop, D.C. Influence of background suppression and retrospective realignment on free-breathing renal perfusion measurement using pseudo-continuous ASL. *Magn. Reson. Med.* **2019**, *81*, 2439–2449. [[CrossRef](#)] [[PubMed](#)]
61. Buxton, R.B.; Uludag, K.; Dubowitz, D.J.; Liu, T. Modeling the hemodynamic response to brain activation. *Neuroimage* **2004**, *23*, S220–S233. [[CrossRef](#)] [[PubMed](#)]

-
62. Kim, S.G.; Ugurbil, K. Comparison of blood oxygenation and cerebral blood flow effects in fMRI: Estimation of relative oxygen consumption change. *Magn. Reson. Med.* **1997**, *38*, 59–65.
 63. Ances, B.M.; Leontiev, O.; Perthen, J.E.; Liang, C.; Lansing, A.E.; Buxton, R.B. Regional differences in the coupling of cerebral blood flow and oxygen metabolism changes in response to activation: Implications for BOLD-fMRI. *Neuroimage* **2008**, *39*, 1510–1521. [[CrossRef](#)] [[PubMed](#)]
 64. Davis, T.L.; Kwong, K.K.; Weisskoff, R.M.; Rosen, B.R. Calibrated functional MRI: Mapping the dynamics of oxidative metabolism. *Proc. Natl. Acad. Sci. USA* **1998**, *95*, 1834–1839. [[CrossRef](#)] [[PubMed](#)]